Quantitative Detection of Biological Nanoparticles in Solution via Their Mediation of Colocalization of Fluorescent Liposomes

Olov Wahlsten,[1] Frida Ulander,[1] Daniel Midtvedt,[1] Måns Henningson,[1] Vladimir P. Zhdanov,[1,2] Björn Agnarsson,[1,*] and Fredrik Höök[1,†]

[1] *Department of Physics, Chalmers University of Technology, SE-412 96 Gothenburg, Sweden*
[2] *Boreskov Institute of Catalysis, Russian Academy of Sciences, Novosibirsk 630090, Russia*

(Received 4 February 2019; revised manuscript received 16 September 2019; published 9 December 2019)

Detection of biomolecules and biological nanoparticles by means of induced aggregation of larger nanoparticles using light scattering as readout was first accomplished in the middle of the last century. Since then, technical advances together with novel nanomaterials have enabled more sophisticated readout schemes, paving the way for methods exploiting dual-probe hybridization for biomolecular or nonoparticle recognition that today can compete with established bioanalytical methods. Herein, we present a quantitative assay, with single-nanoparticle readout, utilizing receptor-containing cell-membrane mimics in the shape of approximately 100-nm lipid liposomes rather than conventional antibody-modified nanoparticles to enable detection of virus particles in solution. Specifically, the method is based on virus-mediated aggregation of differently fluorescent-labeled liposomes that contain the ganglioside GM1 receptor for the Simian Virus 40 (SV40). The aggregation kinetics of the differently colored liposomes is studied by monitoring the spatial colocalization level of the liposomes and a theoretical model that successfully represents aggregation kinetics versus virus concentration is proposed. The limits of detection are identified experimentally for our current setup and theoretically in a more general context. The consistency between theory and experiments suggests that the approach will be generically applicable for similar biosensing applications or for the study of related systems where natural interactions with cell-membrane components can be used to induce liposome aggregation.

DOI: 10.1103/PhysRevApplied.12.064021

I. INTRODUCTION

In the context of the biological sciences, one of the prerogatives of applied physics is the development of methods for the characterization of biomolecules and bionanoparticles in general and measurements of their concentrations in particular. The latter is challenging if the concentration is low. Due to their high specificity and good limits of detection (LODs) when measuring low bulk concentrations of biomarkers (analytes), enzyme-linked immunosorbent assay (ELISA) and polymerase chain reaction (PCR) techniques today dominate the field of biomarker-based clinical diagnostics [1,2]. ELISA achieves high specificity by ensuring signal generation if an analyte of interest simultaneously interacts with two different antibodies, one of which is immobilized on a sensor surface. The other antibody is added after incubation and subsequent rinsing of the analyte and acts as signal transducer through an enzymatic reaction. In PCR, a particular DNA or RNA sequence of interest is detected by producing millions of synthetic copies of the specific sequence, which are then registered using standard fluorescence readout. In the case of virus detection, immunolabeling combined with flow-cytometry-based readout can offer single virus detection and LODs that compete with PCR (in the attomolar regime) [3].

Other formats of surface-based assays, with the added capability of detecting analyte molecules individually, have recently been realized [4]. With nonspecific interactions sufficiently suppressed, the impressive sensitivity offered by these methods has the potential to significantly improve the LOD compared to conventional ELISA formats. The corresponding LOD can be understood by considering the affinity of an interaction between an analyte and an immobilized antibody. In essence, the fraction of antibodies, α (where $0 < \alpha < 1$), on a surface having an analyte bound (at equilibrium) is related to the analyte concentration, C, and the equilibrium dissociation constant, K_d, of the antibody-analyte pair through $\alpha = C/(K_d + C)$. Assuming an antibody-analyte affinity of K_d of 1 nM, the sensitivity in terms of fractional coverage required to detect an analyte concentration of 1 fM is approximately $C/K_d = 10^{-6}$. Hence, since an antibody

*bjornagn@gmail.com
†fredrik.hook@chalmers.se

has a footprint of approximately 10×10 nm^2, about one antibody-analyte complex per 10×10 μm^2 surface area should be detectable. Thus, by monitoring a surface area on the order of 100×100 μm^2, single-molecule sensitivity can yield sufficient statistics (approximately 100 events) to obtain trustworthy LODs in the low-femtomolar regime and even lower.

However, many surface-based assays require multiple washing and addition steps and are, for very low analyte concentrations, significantly hampered by the low rate of analyte diffusion to a planar solid-liquid interface. By instead generating a detectable signal upon complex formation of an analyte directly in solution, as in the mix-and-read protocols of so-called homogeneous immune assays [5], not only are the measurements significantly simplified but the kinetics are also faster compared to surface-based setups. With the exception of quantitative PCR (qPCR) [6], where dye-modified oligonucleotide probes light up upon sequence-specific hybridization to the PCR products, the most common diagnostic solution-based assays make use of physical contrasts induced upon complex formation between suspended antibody-modified beads and free-floating analytes. Commonly, nano-sized to micron-sized beads are modified with two different antibodies directed against different epitopes of an analyte (cf. ELISA), which upon aggregation leads to a change in light scattering [7–10]. Alternative readout principles include changes in solution viscosity [11,12], magnetic properties [13,14], spectral properties based on plasmonic resonance of noble-metal nanoparticles [15–20] or making use of a combination of different readout mechanisms [21]. With one of the interacting partners being fluorescently labeled, fluorescence-correlation spectroscopy (FCS) is another method to probe immunocomplex formation in solution, given that the change in diffusivity upon complex formation is within the detectable range [22].

While convenient from both a preparative and an analytical perspective, homogeneous assays face certain challenges in comparison with surface-based assays such as ELISA; in particular, with respect to reaching low LODs. For example, with the same argumentation as presented above applied to the surface of a bead, on the order of 10^4 antibodies can be allocated on a single bead with a diameter of 0.5 μm. This means that at femtomolar concentrations in equilibrium, only one in every hundred beads will have an analyte bound to it, which in turn means that one must be able to measure very small contrasts using a suitable physical readout property (light scattering, viscosity, magnetic properties, etc.) in order to obtain a LOD that is comparable to that of surface-based methods. In addition, in analogy with ELISA-based detection methods, the high affinity offered by antibodies, which are typically used to reach low LODs, tends to exclude the use of the often much weaker natural ligand-receptor interactions in diagnostics assays of this type. Since antibody recognition must not necessarily represent the functional state of the detected biomolecule, there is a potential advantage in using natural interactions in diagnostic assays.

In this study, we exploit two properties of viruses that make them particularly suitable for homogeneous assays based on specific complex formation between suspended nanoparticles of larger size. First, many viruses have spherical symmetry with multiple ligand sites homogeneously distributed on their surface. Second, albeit each individual ligand-receptor interaction is typically weak (with K_d ranging between micromolar and millimolar), viruses tend to ensure high affinity via multivalent interactions, with multiple receptors on the cell surface during infection [23]. The fact that certain spherically symmetric viruses bind highly specifically to their targets by attaching to multiple glycolipid receptors is used herein for the purpose of designing a homogeneous assay based on virus-induced aggregation of fluorescently labeled glycolipid-containing liposomes.

As a model system for employing this concept for virus detection, we use viruslike particles (VLPs) mimicking Simian Virus 40 (SV40), which in its native form causes infection mediated via binding of the virion protein VP1 to ganglioside GM1 lipids at cellular membranes [24]. Inspired by recently developed methods exploiting dual-probe hybridization to the biomolecular target with a coincidence readout of colocalized differently fluorescently labeled nanoparticles [25], the VLP-mediated formation of liposome dimers and larger aggregates is quantified employing a dual-image microscopy setup that allows for simultaneous probing of the two types of liposomes, aggregates of which are identified using a colocalization image analysis software. In this context, we recall that in normal conditions, the interaction between liposomes is weak [26] and without mediation they do not aggregate and/or fuse [this is well known from, e.g., numerous nanoparticle-tracking analysis (NTA) and dynamic light scattering (DLS) measurements of the liposome size distribution]. The aggregation and fusion are possible but only on a very long time scale (weeks or months), i.e., on time scales much longer than our experiments [27].

The use of fluorescent liposomes as binding reporters has two major advantages over other more conventional antibody-modified nanoparticle reporters, namely that they can be easily functionalized with various recognition elements, the high mobility of which ensures high affinity through the establishment of multiple weak interactions, and that the assay can be easily expanded to many other biological nanoparticles, such as micelles, bicells, and extracellular vesicles (liposomes with complex composition), which have gained in importance as diagnostic markers [28] as well as for exploration of drug-delivery vehicles designed to interact specifically with cell membranes [29].

II. EXPERIMENTAL

A. Materials

Monosialotetrahexosylganglioside lipids from bovine brain (GM1) and 1-palmitoyl-2-oleoyl-sn-glycero-3-phosphocholine (POPC) are purchased from Avanti Polar Lipids, USA. Atto-488-labeled 1,2-dioleoyl-sn-glycero-3-phosphoethanolamine (Atto 488 DOPE) lipids and Atto-633-labeled 1,2-dioleoyl-sn-glycero-3-phosphoethanolamine (Atto 633 DOPE) lipids are purchased from Atto-TEC GmbH, Germany. Recombinant VLP of Simian Virus 40 (SV40) is purchased from abcam, UK. Recombinant cholera toxin B subunit (rCTB) and phosphate-buffered saline (PBS) tablets are purchased from Sigma-Aldrich, Germany.

B. Liposome preparation

Lipid material (98 wt% POPC, 1 wt% GM1 and 1 wt% of either Atto 488 DOPE or Atto 633 DOPE) is dissolved in methanol and mixed and allowed to evaporate at the bottom of a round flask under a gentle stream of N_2. Solvent residues are removed by putting the flask under vacuum for a time exceeding 1 h. The lipid film is then rehydrated with PBS and vigorously vortexed (>1 min) to form vesicular structures. The lipid solution is then extruded 11 times through a 30-nm polycarbonate membrane (Whatman, UK) using a miniextruder (Avanti Polar Lipids, USA). The size distributions of the liposomes (for a detailed size distribution, see Sec. 1 in the Supplemental Material [30]) is measured using NTA (NanoSight, LM10 module, Malvern Instruments Ltd., UK). The spectral characteristics of the liposomes are confirmed using a spectrofluorometer (for excitation and corresponding emission spectra, see Sec. 2 in the Supplemental Material [30]).

The specificity of the interaction between GM1 ganglioside and VLPs is confirmed using quartz-crystal microbalance with dissipation (for a detailed description of the measurements, see Sec. 3 in the Supplemental Material [30]).

C. Microscopy and flow cell

The dual-color fluorescence microscopy measurements are performed on an upright Leica DM LM microscope equipped with a Hamamatsu ORCA-Flash4.0 LT Digital CMOS camera and a water-immersion objective (HCX APO L 63×/0.90 W U-V-I, Leica, Germany). A home-built sample holder is used (see Fig. S4 and associated text in Sec. 4 of the Supplemental Material [30]), consisting of a piece of black-colored polydimethylsiloxane (PDMS) made from a mixture of 10:1 Sylgard 184 and curing agent (Dow Corning, Mid-land, MI) that is rendered nontransparent through the addition of 3 wt% black LEGO® color. A narrow channel ($1.5 \times 1.5 \times 40$ mm^3 with a total volume of approximately 100 μl) is molded into the PDMS and sealed off with a rectangular cover-glass slide (No. 1), leaving just a sample inlet and outlet. Through an incision in the PDMS, a multimode optical fiber (0.22 NA, 50 μm core diameter, Thorlabs, Germany) is introduced, allowing for the excitation of the fluorescently labeled liposomes in the channel right under the objective.

D. Experimental procedure

Direct excitation of both types of fluorophores is enabled using monochromatic light from two different lasers that are simultaneously guided through the multimode fiber into the sample chamber. The wavelengths of the lasers used are as follows: 488 nm (maximum power: 150 mW, Cobolt, Germany) and 635 nm (maximum power: 20 mW, OZ-3000, OZ Optics, Canada). The fluorescent emission from the labeled liposomes is collected by the objective and passed through an image splitter (W-VIEW GEMINI, Hamamatsu) to enable monitoring of the two types of fluorescently labeled liposomes simultaneously and separately. The image splitter is equipped with a long-pass filter [transmission (Tr) $>$ 560 nm, Semrock Inc.] and two fluorescence filters (535/50 nm and 700/75 nm, Chroma Technology Corporation), as illustrated in Fig. 1. Images are acquired at approximately 30 frames/s (2×2 binning) at a 33-ms exposure time with a laser power of 5 mW (488-nm laser) and 10 mW (635-nm laser). The insets in Fig. 1 show the resulting micrographs of suspended liposomes (0.33 pM of each color after dilution) simultaneously imaged in the green and red channels after 60 min of incubation with SV40 VLPs (100 pM) and subsequent dilution ($\times 10$). The particular liposome concentration (0.67 pM) is used for all measurements, since it allows for liposomes and aggregates to be easily distinguished on an individual level. At higher concentrations, individual objects become difficult to distinguish, while at lower liposome concentrations, the total number of liposomes and detected aggregates is too low to obtain good statistics. The buffer used throughout all experiments is PBS.

E. Image analysis

Custom-written scripts (MATLAB R2014b, MathWorks Inc.) are used to determine the colocalization level for each individually recorded movie (1000 frames, 1024×1024 pixels per frame, including both fluorescence channels). First, the two fluorescence channels are mapped onto each other and aligned to compensate for any possible spatial aberration due to optical imperfections in the instrumental setup (for additional details on the channel alignment, see Sec. 5 A in the Supplemental Material [30]). After background removal, all objects, both overlapping (colocalized aggregates containing at least one liposome of each color) and nonoverlapping (all aggregates and monomers), in each channel are identified (for a detailed description of the identification of the colocalized objects, see Sec.

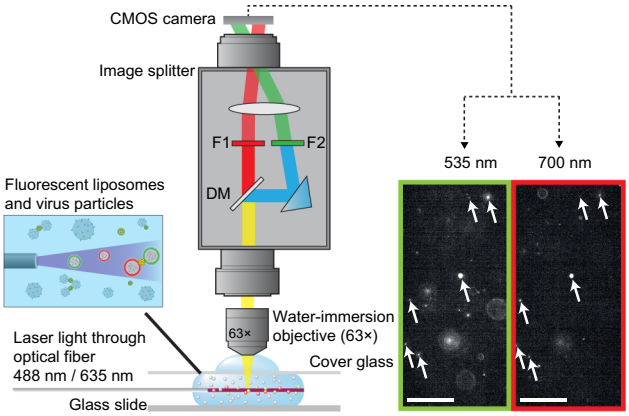

FIG. 1. A schematic illustration of the dual-color fluorescence microscopy setup used for the detection of virus particles. Ganglioside-containing liposomes labeled either with Atto 633 (red) or Atto 488 (green) PE lipids are used as color-coded reporters. An optical multimode fiber, simultaneously guiding laser light of two different wavelengths, inserted into the sample chamber allows for direct excitation of the fluorescent liposomes. The emitted light from the liposomes is collected by an objective positioned perpendicularly to the illumination path and guided via an image splitter, composed of a dichroic mirror (DM, Tr $>$ 560 nm) and two fluorescence filters (F1 $=$ 700/75 nm and F2 $=$ 535/50 nm), onto different parts of a CMOS camera. The insets show two different types of fluorescently labeled liposomes individually distinguished in the same field of view using the dual-color microscopy setup. Colocalized liposomes (aggregates consisting of at least one entity of each fluorescent liposome) are identified from overlays of the images (indicated with white arrows). The scale bars are 50 μm.

5 B in the Supplemental Material [30]). Finally, the ratio between the total intensity of all colocalized objects and the total intensity of all identified objects is computed for both channels, with the colocalization level defined as the mean ratio from the two channels (for details about how the colocalization level is calculated, see Sec. 5 C in the Supplemental Material [30]).

III. RESULTS AND DISCUSSION

A. Detection principle by colocalization

Aggregation is a general process that occurs under different conditions ranging from supersaturation in gas phase to the formation of capsids during virion replication in cells. Customarily, it is described by a set of kinetic equations for populations of aggregates formed from different numbers of monomers (two good examples here are the classical nucleation theory [31] and numerous models of protein aggregation [32]; for other examples, see the review in Ref. [33] and several recent articles [34–36] and the references therein). Such equations are usually cumbersome even if the process includes attachment and detachment of monomers of only one type. In our case, the aggregation of monomers of one type (GM1-containing liposomes) is mediated by monomers of the other type (SV40 VLPs) and the monomers of both types are distributed over size. Models treating aggregation under such conditions are lacking. In our analysis (Fig. 2), we focus on the aggregation of particles of one size (liposomes) induced by particles of another size (VLPs) and ignore the distribution of liposome and VLP sizes, since these distributions are not wide. In particular, we operate with the average sizes (diameters) of liposomes (110 nm) and viruses (40 nm). Each liposome of this size (with radius $r = 55$ nm) is considered to possess N effective sites for VLP attachment, each with an area of $(4\pi r^2/N)$. Each site can be vacant or irreversibly occupied by one VLP. After binding to an attachment site on one liposome, a VLP can irreversibly attach to a vacant site on a different liposome and form a liposome dimer. We can thus identify three types of populations of attachment sites, with the following concentrations: s_E (empty attachment site); s_{FA} (occupied attachment site and available for mediation with a different binding site); and s_{FNA} (occupied attachment site, forming a bond between two liposomes and nonavailable for further mediation). Attachment sites that are empty and nonavailable are not considered in this model since they require some shadowing effect to take place, which does not seem to be likely due to the appreciable difference between the liposome and VLP sizes.

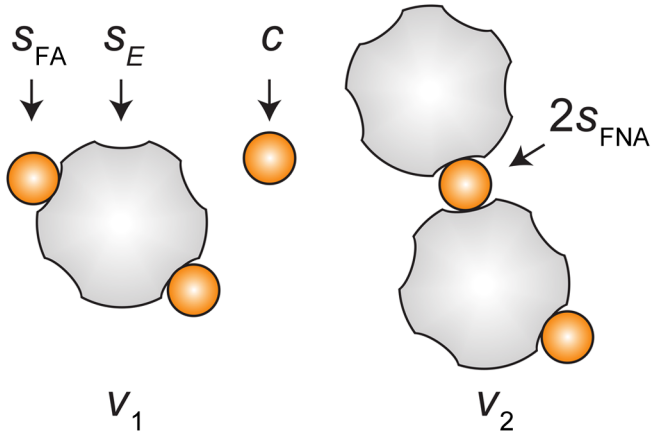

FIG. 2. The scheme of the arrangements of reactants, including a liposome with two bound VLPs (left), an unbound VLP (middle), and two liposomes aggregated via a VLP (right). s_{FA}, s_E, s_{FNA}, c, v_1, and v_2 are the corresponding concentrations. In these designations, "FA," "E," and "FNA" are abbreviations of "filled available," "empty," and "filled nonavailable," respectively. "2" is added to "s_{FNA}" to indicate that there are two filled (one on each liposome) and nonavailable sites. In general, the populations of liposome aggregates (dimers, trimers, etc.) are indexed according to how many liposomal monomers they contain (v_1, v_2, and so on). For visualization, the attachment sites are shown as recesses on the liposome surface.

The experimental results indicate that the VLP-mediated liposome aggregation is a kinetically limited association process. This is based on the dose-response curves (Fig. 4), which would, in a diffusion-limited association process, be shifted more toward lower VLP concentrations (simulated, but not shown). For a kinetically limited association process, the association rate is proportional to the effective contact area of the interacting objects. In solution, this contact area can be represented as $4\pi(r_1+r_2)^2$, where r_1 and r_2 are the radii of the two interacting objects. While the aggregates formed in this system may not be entirely spherical, since, on the time scale of the whole measurement, the lipid diffusion in the liposomes is fast, the number of VLP-mediated contacts is expected to be maximized. Hence, the aggregates formed can be approximated as close packed. With this in mind we can assume that the radii of two associating aggregates are proportional to $n_1^{1/3}$ and $n_2^{1/3}$, where n_1 and n_2 are the numbers of liposomal monomers in the associating aggregates. Neglecting the VLP size (because it is small compared to the liposome size), the contact area between two associating liposomal aggregates can be defined as $4\pi r^2(n_1^{1/3}+n_2^{1/3})^2$, where r is the radius of a monomeric liposome. Then, the liposome-liposome association rate can be expressed as

$$W=\xi 4\pi r^2(k^{1/3}+p^{1/3})^2\frac{s_E}{s_0}\frac{s_{\mathrm{FA}}}{s_0}v_k v_p, \tag{1}$$

where ξ is the effective relative velocity of vesicles or aggregates upon crossing the contact area, indices k and p represent the size of each liposome aggregate (expressed in units of monomers), and s_E/s_0 and s_{FA}/s_0 are the probabilities that an attachment site is available or occupied but available for mediating the aggregation (s_0 is the total concentration of attachment sites in the system). The crossing takes place locally during the liposome-liposome contact and physically it is primarily related to the motion of the VLP that mediates the process. For this reason, ξ is expected to be independent of the liposome size. A suitable scale for expressing ξ is D_{VLP}/ρ, where D_{VLP} is the diffusion coefficient of the VLP in solution and ρ is its radius. Using this scale, one can write $\xi=q_2 D_{\mathrm{VLP}}/\rho$, where q_2 is a dimensionless factor, taking into account that in reality ξ is smaller than D_{VLP}/ρ, because the attachment itself may occur with an activation barrier that is somewhat higher than that for diffusion. With this expression for ξ, Eq. (1) can be rewritten as

$$W=q_2 k_*(k^{1/3}+p^{1/3})^2\frac{s_E}{s_0}\frac{s_{\mathrm{FA}}}{s_0}v_k v_p, \tag{2}$$

where

$$k_*=\frac{4\pi r^2 D_{\mathrm{VLP}}}{\rho}. \tag{3}$$

Equations (1) and (2) are valid for $k\neq p$. For $k=p$, the reactants are indistinguishable and, accordingly, these expressions used formally imply that each contact is considered twice (compared to $k\neq p$), i.e., they should be divided by 2. In our presentation below, the latter factor is ignored in order to keep the equations compact. If necessary, it can be taken into account but, ultimately, it will not affect the conclusions.

To describe the association of VLPs with liposomes, it is convenient to use the concentration of available sites of attachment. The corresponding association-rate constant should describe association with a single attachment site. As a measure of this rate constant, we use k_*/N, where N is introduced to renormalize k_* to a single attachment site. Then, the rate constant is represented as $q_1 k_*/N$, where the dimensionless constant of proportionality q_1 is introduced to account for the fact that an encounter between a VLP and an available attachment site does not always lead to successful binding.

With the specification given above, the equations describing the time-evolution of the concentrations defined in the caption of Fig. 2 are as follows:

$$\frac{dc(t)}{dt}=-q_1 k_* N^{-1}c(t)s_E(t), \tag{4}$$

$$\frac{ds_E(t)}{dt}=\frac{dc(t)}{dt}-\frac{1}{2}\frac{ds_{\mathrm{FNA}}(t)}{dt}, \tag{5}$$

$$\frac{ds_{\mathrm{FA}}(t)}{dt}=-\frac{dc(t)}{dt}-\frac{1}{2}\frac{ds_{\mathrm{FNA}}(t)}{dt}, \tag{6}$$

$$\frac{ds_{\mathrm{FNA}}(t)}{dt}=2\sum_{kp}W_{kp\to k+p}, \tag{7}$$

$$\sum W_{kp\to k+p}=q_2 k_*(k^{1/3}+p^{1/3})^2\times\frac{s_E(t)}{s_0}\frac{s_{\mathrm{FA}}(t)}{s_0}v_k(t)v_p(t), \tag{8}$$

$$\frac{dv_n(t)}{dt}=-2\sum_{k=n}W_{kn\to k+n}-\sum_{k\neq n}W_{kn\to k+n}+\sum_{k<n}W_{k(n-k)\to n}. \tag{9}$$

At $t=0$, the aggregation is considered to be negligible. The corresponding initial conditions are $c(0)=c_0$, where c_0 is the total concentration of VLPs (bound and free); $v_1(0)=v_0$, where v_0 is the total concentration of liposomes (disregarding the aggregation); and $v_i(0)=0$ for $i>1$. The largest aggregates considered in the calculations are decamers (v_{10}). Allowing for even larger aggregates has an insignificant effect on the final results (data not shown). The number of sites for VLP attachment is set to 10 (i.e., $N=10$).

We assume that the rate constants introduced are the same irrespective of liposome color and, accordingly, operate with the whole liposome concentration. If two populations of liposomes of different colors are used, the two colors of the liposomes in the aggregates will be randomly distributed. In particular, the probability that an i-mer contains liposomes of only one color is equal to $(1/2)^{i-1}$, assuming an equal number of liposomes of each color in solution. The probability that an i-mer contains at least one liposome of each color is accordingly given by

$$p_{\mathrm{col}}(i) = 1 - (1/2)^{i-1}. \tag{10}$$

From an experimental point of view, the latter probability can be identified with the measured colocalization probability [which explains the choice of the subscript in Eq. (10)]. Also, by analogy with the experiment, the colocalization level (in %) of the whole system can be defined as the fraction of i-mers containing at least one liposome of each color:

$$F(t) = 100 \sum_{i\geq 1}^{10} v_i(t) p_{\mathrm{col}}(i) \Bigg/ \sum_{i\geq 1}^{10} v_i(t)\ . \tag{11}$$

This expression makes it possible to compare the predictions of the theoretical model with the experimental data.

B. Measurement procedure

A dual-color fluorescence microscopy setup (see Sec. II) is used to spatially resolve SV40-VLP-induced aggregation of differently labeled fluorescent liposomes [50% of the liposomes containing Atto 488 DOPE (green) and 50% Atto 633 DOPE (red)]. The liposomes are illuminated with semicollimated light of two wavelengths (488 nm and 635 nm), guided through a single fiber, and their emission is imaged on two adjacent regions of a CMOS camera after passing an image splitter.

C. Temporal evolution of the colocalization level

The measured temporal evolution of the colocalization level [Fig. 3(a)] exhibits a gradual increase that reaches a colocalization level of around 60%, meaning that just over half of all liposomes are engaged in complexes with at least two-colored liposomes after 120 min of incubation. The experimental data can be fitted with the model given by Eqs. (4)–(9) [red curve in Fig. 3(a)] and a heat map showing the squared deviations of the two fitting parameters, q_1 and q_2 [the inset in Fig. 3(a)]. The white dot indicates the parameter combination resulting in the smallest error, which in addition to the q_1 and q_2 parameters is represented by a distribution in the number of aggregates of each size. The green bars in Fig. 3(b) represent the distribution of monomers, dimers, tetramers, etc., using the same parameters as obtained from the fit represented in Fig. 3(a) at equilibrium (100 pM VLPs, 6.7 pM vesicles, and $t = 90$ min). The blue bars represent the statistically expected fraction of aggregates composed of liposomes containing both colors [Eq. (10)]. Neglecting the influence of the VLP itself, the hydrodynamic radius of a fractal aggregate formed from N identical spherical liposomes can be roughly represented as [37]

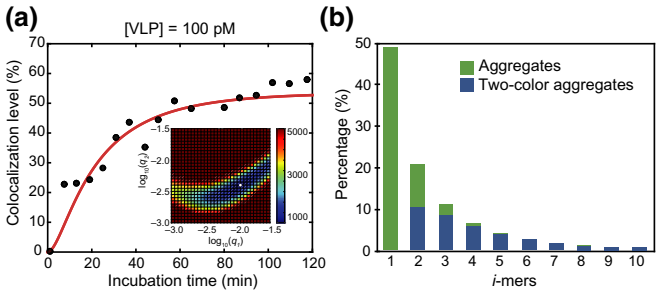

FIG. 3. (a) The measured colocalization level versus the incubation time for a solution containing 3.3 pM green-labeled and 3.3 pM red-labeled liposomes and 100 pM SV40 VLPs. The incubating solution is diluted 10 times prior to measuring. In this case, the colocalization of just under approximately 60%, observed at the end of the measurements, corresponds on average to approximately two liposomes per aggregate. The inset shows a heat map of the squared deviation between the model and the experimental data for different combinations of the q_1 and q_2 parameters of the model. The best fit is achieved for parameters $q_1 = 0.0112$ and $q_2 = 0.004$ (indicated with a white dot in the inset). (b) The model prediction of the distribution of aggregates irrespective of their color (green) and two-color aggregates (blue) as a function of i-mers at equilibrium ($t = 90$ min) for $q_1 = 0.0112$ and $q_2 = 0.004$.

$$R \propto r N^{1/d_f}\,, \tag{12}$$

where r is the hydrodynamic radius of a monomeric liposome and d_f is the fractal (Hausdorff) dimension, which for reaction-limited cases is approximately 2.1 [38–40]. Using the distribution of aggregates shown in Fig. 3(b), one obtains an average aggregate radius of $1.4r$, which is in excellent agreement with the average aggregate size measured at equilibrium using NTA [40% increase in mean diameter (data not shown)].

D. VLP dose response

Although the model can represent the experimental data fairly well [Fig. 3(a)], it is obvious from the heat map that there is a fairly broad interval of combinations of q_1 and q_2 that yield reasonably good fits. To gain further insight into the kinetics of the SV40-VLP-induced liposome aggregation, dose-response curves are measured in a broad concentration interval of SV40 VLP (femtomolar to nanomolar) for 30 min [Fig. 4(a)] and 90 min

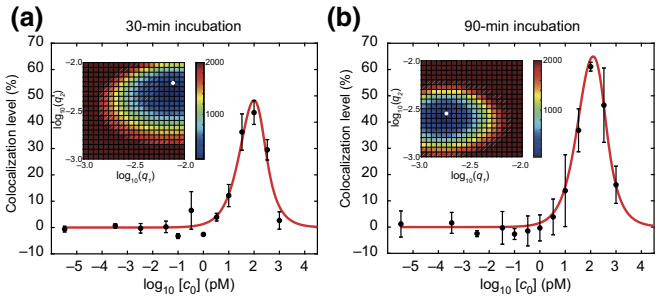

FIG. 4. The VLP-mediated colocalization level as a function of the initial VLP concentration (c_0) after (a) 30 min and (b) 90 min of incubation. The data points are mean values and the error bars represent the standard deviation of three independent measurements. To quantify the colocalization level, the contribution from random overlaps between freely diffusing liposomes or nonspecifically interacting liposomes is evaluated and subtracted from the results. The average colocalization level measured for VLP concentrations $\leq$100 fM is considered as the background colocalization level, which is subtracted from all data points. The insets show the squared deviation between the experimental data and the model for different combinations of q_1 and q_2. The smallest deviations (indicated with white circles) are obtained for $q_1 = 0.008$ and $q_2 = 0.006$ at 30 min of incubation and $q_1 = 0.002$ and $q_2 = 0.003$ at 90 min of incubation, respectively.

[Fig. 4(b)] of incubation at a fixed total liposome concentration of 6.7 pM (3.3 pM green-labeled liposomes and 3.3 pM red-labeled liposomes). Also shown are the best fits to the model (the red solid curve) and the corresponding heat maps of the squared deviations between the experimental data and the model (the insets). Statistically, significant detection of colocalization is observed at a VLP concentration of approximately 2 pM, after which the colocalization level gradually increases until it peaks at approximately 45% and approximately 65% for 30- and 90-min incubation times, respectively, for a VLP concentration of approximately 100 pM. At higher concentrations, there is a drastic reduction in the colocalization level, which is attributed to the "high-dose Hook effect" [41], which occurs when the VLP concentration becomes so high that individual liposomes get completely covered with VLPs and thus prevents them from forming aggregates.

From the heat maps illustrating the ability of the proposed theoretical model to represent the experimental data, it is interesting to note that in both cases, fairly small intervals for q_1 and q_2 give reasonable fits. However, in agreement with the time-resolved data [Fig. 3(a)], the uncertainty is larger for q_1, which, if all data sets are included, appears in an interval from approximately 0.002 to 0.011, while q_2 appears to be in a narrow interval from 0.003 to 0.006. These values of q_1 and q_2 indicate that, as one could expect, the processes under consideration occur with fairly low activation energies, $\Delta E_{\rm act}$, on the scale of 3 kcal/mol [note that this value, obtained via $q_2 = \exp(-\Delta E_{\rm act}/k_B T)$, is additional to the activation energy characterizing $D_{\rm VLP}$, because according to Eq. (3), k_* is expressed via $D_{\rm VLP}$]. While q_1 is introduced in the model as a dimensionless proportionality constant simply to account for the fact that an encounter between a VLP and an available attachment site on a liposome does not always lead to successful binding, information about the value of q_2 can be used to estimate the velocity, $\xi = q_2 D_{\rm VLP}/\rho$, characterizing the bond formation during contacts [see the text below Eq. (1)]. For the obtained interval of q_2, this velocity ranges from 1.5 to 3.0 μm/s.

IV. ON THE LIMIT OF DETECTION

It is interesting to investigate how many false-positive readings one might expect to obtain using our current configuration. False positives are obtained when two liposomes of opposite color are found at the same place at the same time by coincidence. In our analysis, we consider that nanoparticles of interest mediate colocalization of fluorescent microscale and/or nanoscale tracers of two colors. The unbound tracers are considered to be located at random. The concentration of tracers of each color is C. The size of nanoparticles is appreciably smaller than that of tracers. Our goal is to determine the nanoparticle concentration, c, by measuring the number of aggregates containing colocalized tracers of different colors. This number is assumed to be measured in the region with frontal area S (defined by the field of view) and thickness H (defined by the depth of focus). The volume of this region is HS and one can safely assume that $H \ll S^{1/2}$.

To start, let us consider that: (i) a nanoparticle is able to colocalize only two tracer particles, so that the subsequent colocalization of such dimers is impossible; (ii) the colocalization is irreversible; and (iii) C is appreciably larger than c, so that all the nanoparticles are bound. In this case, on average, the region under consideration contains $cHS/2$ dimers formed by tracers of different colors. To measure this number reliably by making N snapshots, one is expected to satisfy two necessary conditions. First, the total average number of dimers formed by tracers of different colors and detected during the measurements should be appreciable, $cHSN/2 \gg 1$, or

$$c \gg 2/(HSN). \tag{13}$$

With regard to this condition, we add that the interval between the snapshots, τ, should be long compared to the time scale of the dimer diffusion perpendicular to the frontal area, i.e.,

$$\tau \gg H^2/D, \tag{14}$$

where D is the diffusion coefficient. The latter condition guarantees that the snapshots are physically different.

Second, the average number of double-color dimers, $cHS/2$, observed at each snapshot should be appreciably larger than the number of dimers apparently formed by tracers of different colors due to occasional coincidence of their locations if they are frontally observed. To calculate the latter number, we take into account that the average number of tracers of each color is CHS. If ρ is the radius (maximum of the tracer diameter, d, and the wavelength used, λ) of the $2D$ indistinguishability region, the probability that a tracer of one color has at least one tracer of another color apparently observed nearby is given by the Poissonian distribution,

$$p = 1 - \exp(-\pi\rho^2 HC). \tag{15}$$

At practically important conditions, one is expected to have

$$\pi\rho^2 HC \ll 1 \tag{16}$$

and Eq. (15) can be expanded and replaced by

$$p \simeq \pi\rho^2 HC. \tag{17}$$

Multiplying CHS and p yields the number of dimers apparently formed by tracers of different colors, $\pi\rho^2 H^2 SC^2$. As already noted, this number should be much smaller than $cHS/2$, i.e., one should have

$$c \gg 2\pi\rho^2 HC^2. \tag{18}$$

If the nanoparticles of interest mediate the formation of aggregates of fluorescent microscale and/or nanoscale tracers, the situation becomes more complex and one should operate with the aggregate distribution. For a rough orientation, it makes, however, sense to analyze this situation at the coarse-grained level by operating with the average number of nanoparticles, $\langle n\rangle$, per aggregate. In this case, almost every aggregate contains tracers of different colors, the concentration of aggregates is approximately equal to $c/\langle n\rangle$, and the condition given by Eq. (13) can be rewritten as

$$c \gg 2\langle n\rangle/(HSN). \tag{19}$$

If $\langle n\rangle$ is not too large (e.g., smaller or comparable with 10, as it is expected to be), we can still use the relation (17) in order to obtain the second condition (because the aggregate size is weakly dependent on n). According to this approximation, the number of dimers apparently formed by tracers of different colors is again given by $\pi\rho^2 H^2 SC^2$. This number should be much smaller than $cHS/\langle n\rangle$ and, accordingly, condition (18) can be rewritten as

$$c \gg \pi\rho^2 HC^2\langle n\rangle. \tag{20}$$

The right-hand sides of conditions (13) and (18) for dimers or conditions (19) and (20) for larger aggregates determine the limit of detection of nanoparticles. In particular, the nanoparticle concentration should be at least 10 times larger than the maximum value given by these conditions.

To put these conditions into perspective, the depth of field (H) in our experimental setup is determined by the $63\times$, NA $= 0.9$ objective and is on the order of 1000 nm. ρ is equal to a longer emission wavelength (approximately 650 nm) and $\langle n\rangle$ is between 2 and 10, approximately. In our measurements, the concentration of tracer vesicles during imaging is at $C = 0.33$ pM for each color. Using these values with relation (20) gives

$$c \gg 1 \times 10^{-6}\,\text{nM}. \tag{21}$$

The assumption that the nanoparticle concentration should be at least 10 times larger than this value results in

$$c > 1 \times 10^{-5}\,\text{nM}. \tag{22}$$

According to these calculations, false-positive events, due to coincidental spatial and temporal overlap between two objects of different colors in our system, should not be considerable for nanoparticle concentrations (viruses in our case) above the 10^{-14} M regime. However, as will be discussed in Sec. V, practical limitations with the detection algorithm and possible nonspecific binding between liposomes of different colors will act to increase this theoretical value.

Given the ability of the proposed theoretical model to represent the kinetics of VLP-induced liposome aggregation, it is instructive to employ it to predict the expected colocalization level at ultralow virus concentrations under the assumption that the nonspecific liposome association is fully suppressed. Interestingly, with q_1 and q_2 values in the interval obtained from the fits shown in Figs. 3 and 4, at a VLP concentration of 3 fM, the expected colocalization level would be only approximately 0.01% after 30 min of incubation, i.e., 1 in every 10 000 detected events would be colocalized. With the current setup, it is possible to clearly distinguish approximately 25 liposomes in the field of view, which on average remain there for approximately 10–20 s. This means that within 30 min, no more than approximately 3000 liposomes can be imaged, resulting in a practical LOD on the order of approximately 30 fM. To gain better statistics and improve the LOD, a flow system could be implemented, which would increase the number of detected liposomes per time unit. Additionally, active mixing by stirring during incubation could also speed up the aggregation process, which would yield increased colocalization within the same incubation time. The measured

LOD of around a few picomolars is still about 50 times higher than the practical limit of about 30 fM, a discrepancy that can be attributed to limitations in the detection algorithm and to possible nonspecific interactions between liposomes.

V. CONCLUSIONS

We present a quantitative solution-based bioanalytical assay for the detection of virus particles, reaching a limit of detection in the low-picomolar range within 30 min. As the readout mechanism is based on the detection of individual aggregates of fluorescently labeled liposomes of different types, detection can in principle be achieved as soon as a single colocalized pair (composed of liposomes of different color) can be identified in the field of view. From a theoretical point of view, the LOD is governed by false-positive errors due to colocalized events occurring by coincidence. For liposome concentrations used in our measurements of 6.7 pM, the corresponding theoretical LOD, assuming the unbound vesicles to be located at random, approximately equals 10^{-2} pM, which is similar to the best LODs previously reported for homogeneous assays of this type [25] and about 2 orders of magnitude lower than we observe. Thus, other effects, such as possible nonspecific binding of liposomes and limitations in the detection algorithm, contribute in our case to the observed LOD. Two possible ways of reducing false positives in our system and to improve the limit of detection are to: (i) introduce a small fraction of PEG-conjugated lipids to the liposomes, as PEG is known to suppress nonspecific liposome-liposome interactions [42]; and (ii) further improve and develop the image-analysis software, making it capable of distinguishing transient from irreversibly formed aggregates, for example by monitoring the spatiotemporal correlation between events recorded in the two color channels.

It should also be emphasized that the use of fluorescent liposomes as binding reporters has at least two key advantages over other more conventional antibody-modified nanoparticle reporters, namely that they can be easily functionalized with various recognition elements, the high mobility of which ensures high affinity through the establishment of multiple weak interactions, and the fact that the assay can be easily expanded to many other biological nanoparticles, such as micelles, bicelles, extracellular vesicles, or other types of lipid nanoparticles. Further, the use of fluorescent liposomes adds an extra versatility to the assay since, in addition to various lipids, they can host not only conventional recognition elements such as DNA and antibodies but also membrane proteins, or even be made directly from native cell membranes. These recognition elements are mobile on the liposomes, meaning that detection can be achieved even in situations in which there are only a few recognition elements per liposome. Further, the fluorescence readout should also enable molecular detection in crude body samples as long as the nonspecific interaction with the reporter liposomes is suppressed. Additionally, since the method is solution based, it circumvents the need for careful surface cleaning and functionalization protocols as required in corresponding surface-based assays such as surface-plasmon resonance, quartz-crystal microbalance, and ELISA. Since the model developed to account for the kinetics of VLP-induced liposome aggregation is shown to capture the essential features of the measured temporal evolution and the dose-response curves of the aggregation, we also foresee that it will be valuable for the optimization of bioanalytical assays of this type *in silico*.

Finally, we note that although our presentation is written from the perspective of analytical nano- and/or biochemistry, the experimental and theoretical results are of intrinsic interest since they present an instructive example of aggregation of nanoparticles of one type mediated by smaller nanoparticles of other types. Potentially, systems exhibiting kinetics belonging to this class can be encountered in various fields, far beyond biophysical chemistry.

ACKNOWLEDGMENTS

This project was funded by the Swedish Research Council (VR), the Swedish Governmental Agency for Innovations Systems (VINNOVA), and the Göran Gustafsson Foundation.

[1] H. A. Erlich, Polymerase chain-reaction, J. Clin. Immunol. **9**, 437 (1989).
[2] R. M. Lequin, Enzyme immunoassay (EIA)/enzyme-linked immunosorbent assay (ELISA), Clin. Chem. **51**, 2415 (2005).
[3] M. M. Bonar and J. C. Tilton, High sensitivity detection and sorting of infectious human immunodeficiency virus (HIV-1) particles by flow virometry, Virology **505**, 80 (2017).
[4] S. Chen, M. Svedendahl, R. P. Van Duyne, and M. Kall, Plasmon-enhanced colorimetric ELISA with single molecule sensitivity, Nano Lett. **11**, 1826 (2011).
[5] E. F. Ullman, Homogeneous immunoassays: Historical perspective and future promise, J. Chem. Educ. **76**, 781 (1999).
[6] C. A. Heid, J. Stevens, K. J. Livak, and P. M. Williams, Real time quantitative PCR, Genome Res. **6**, 986 (1996).
[7] D. J. Newman, H. Henneberry, and C. P. Price, Particle enhanced light-scattering immunoassay, Ann. Clin. Biochem. **29**, 22 (1992).
[8] I. Delfino, Light scattering methods for tracking gold nanoparticles aggregation induced by biotin-neutravidin interaction, Biophys. Chem. **177**, 7 (2013).
[9] A. Mauceri, S. Borocci, L. Galantini, L. Giansanti, G. Mancini, A. Martino, L. S. Manni, and C. Sperduto, Recognition of concanavalin a by cationic glucosylated liposomes, Langmuir **30**, 11301 (2014).

[10] A. E. James and J. D. Driskell, Monitoring gold nanoparticle conjugation and analysis of biomolecular binding with nanoparticle tracking analysis (NTA) and dynamic light scattering (DLS), Analyst **138**, 1212 (2013).
[11] H. W. Yu, Y. S. Wang, Y. Li, G. L. Shen, H. L. Wu, and R. Q. Yu, One step highly sensitive piezoelectric agglutination method for cholera toxin detection using GM1 incorporated liposome, Procedia Environ. Sci. **8**, 248 (2011).
[12] H. Chen, J. H. Jiang, Y. F. Li, T. Deng, G. L. Shen, and R. Q. Yu, A novel piezoelectric immunoagglutination assay technique with antibody-modified liposome, Biosens. Bioelectron. **22**, 993 (2007).
[13] I. Koh, R. Hong, R. Weissleder, and L. Josephson, Nanoparticle-target interactions parallel antibody-protein interactions, Anal. Chem. **81**, 3618 (2009).
[14] J. M. Perez, F. J. Simeone, Y. Saeki, L. Josephson, and R. Weissleder, Viral-induced self-assembly of magnetic nanoparticles allows the detection of viral particles in biological media, J. Am. Chem. Soc. **125**, 10192 (2003).
[15] N. T. K. Thanh and Z. Rosenzweig, Development of an aggregation-based immunoassay for anti-protein A using gold nanoparticles, Anal. Chem. **74**, 1624 (2002).
[16] C. A. Mirkin, R. L. Letsinger, R. C. Mucic, and J. J. Storhoff, A DNA-based method for rationally assembling nanoparticles into macroscopic materials, Nature **382**, 607 (1996).
[17] J. Khodaveisi, S. Dadfarnia, A. M. H. Shabani, and D. Saberi, Colorimetric determination of nabumetone based on localized surface plasmon resonance of functionalized gold nanoparticles as a chemical sensor, Sens. Actuators B: Chem. **239**, 1300 (2017).
[18] S. Hwang, K. Ha, K. Guk, D. Lee, G. Eom, S. Song, T. Kang, H. Park, J. Jung, and E. Lim, Rapid and simple detection of Tamiflu-resistant influenza virus: Development of oseltamivir derivative-based lateral flow biosensor for point-of-care (POC) diagnostics, Sci. Rep. **8**, 12999 (2018).
[19] W. Qu, Y. Liu, D. Liu, Z. Wang, and X. Jiang, Copper-mediated amplification allows readout of immunoassays by the naked eye, Angew. Chem. Int. Ed. **50**, 3442 (2011).
[20] M. J. Marín, A. Rashid, M. Rejzek, S. A. Fairhurst, S. A. Wharton, S. R. Martin, J. W. McCauley, T. Wileman, R. A. Field, and D. A. Russell, Glyconanoparticles for the plasmonic detection and discrimination between human and avian influenza virus, Org. Biomol. Chem. **11**, 7101 (2013).
[21] L. Xiong, X. He, Z. Zhao, R. Kwok, Y. Xiong, P. Gao, F. Yang, Y. Huang, H. Sung, I. Williams, J. Lam, J. Cheng, R. Zhang, and B. Tang, Ultrasensitive virion immunoassay platform with dual-modality based on a multifunctional aggregation-induced emission luminogen, ACS Nano **12**, 9549 (2018).
[22] C. Xie, C. Q. Dong, and J. C. Ren, Study on homogeneous competitive immune reaction by fluorescence correlation spectroscopy: Using synthetic peptide as antigen, Talanta **79**, 971 (2009).
[23] M. Mammen, S. K. Choi, and G. M. Whitesides, Polyvalent interactions in biological systems: Implications for design and use of multivalent ligands and inhibitors, Angew. Chem. Int. Ed. **37**, 2754 (1998).
[24] M. Schelhaas, J. Malmstrom, L. Pelkmans, J. Haugstetter, L. Ellgaard, K. Grunewald, and A. Helenius, Simian virus 40 depends on ER protein folding and quality control factors for entry into host cells, Cell **131**, 516 (2007).
[25] A. Agrawal, C. Y. Zhang, T. Byassee, R. A. Tripp, and S. M. Nie, Counting single native biomolecules and intact viruses with color-coded nanoparticles, Anal. Chem. **78**, 1061 (2006).
[26] S. Ohki and H. Ohshima, Interaction and aggregation of lipid vesicles (DLVO theory versus modified DLVO theory), Colloids Surf. B: Biointerfaces **14**, 27 (1999).
[27] V. Guida, Thermodynamics and kinetics of vesicles formation processes, Adv. Colloid Interface Sci. **161**, 77 (2010).
[28] S. L. N. Maas, X. O. Breakefield, and A. M. Weaver, Extracellular vesicles: Unique intercellular delivery vehicles, Trends Cell Biol. **27**, 172 (2017).
[29] M. W. Tibbitt, J. E. Dahlman, and R. Langer, Emerging frontiers in drug delivery, J. Am. Chem. Soc. **138**, 704 (2016).
[30] See the Supplemental Material at http://link.aps.org/supplemental/10.1103/PhysRevApplied.12.064021 for liposome size distributions, excitation and/or emission spectra, the schematics of the dual-color fluorescence microscopy setup, the quartz-crystal microbalance with dissipation data, and details on image analysis, which include Refs. [43–45].
[31] V. Kalikmanov, *Nucleation Theory*, Series: Lecture Notes in Physics Vol. 860 (Springer, Dordrech, 2013).
[32] A. M. Morris, M. A. Watzky, and R. G. Finke, Protein aggregation kinetics, mechanism, and curve-fitting: A review of the literature, Biochim. Biophys. Acta Proteins Proteomics **1794**, 375 (2009).
[33] F. Leyvraz, Scaling theory and exactly solved models in the kinetics of irreversible aggregation, Phys. Rep. Rev. Sect. Phys. Lett. **383**, 95 (2003).
[34] J. Szavits-Nossan, K. Eden, R. Morris, C. MacPhee, M. Evans, and R. Allen, Inherent Variability in the Kinetics of Autocatalytic Protein Self-Assembly, Phys. Rev. Lett. **113**, 098101 (2014).
[35] T. Michaels, A. Dear, J. Kirkegaard, K. Saar, D. Weitz, and T. Knowles, Fluctuations in the Kinetics of Linear Protein Self-Assembly, Phys. Rev. Lett. **116**, 258103 (2016).
[36] N. Valadez-Perez, Y. Liu, and R. Castaneda-Priego, Reversible Aggregation and Colloidal Cluster Morphology: The Importance of the Extended Law of Corresponding States, Phys. Rev. Lett. **120**, 248004 (2018).
[37] L. Gmachowski, Calculation of the fractal dimension of aggregates, Colloids Surfaces A: Physicochem. Eng. Aspects **211**, 197 (2002).
[38] W. V. Saarloos, On the hydrodynamic radius of fractal aggregates, Phys. A: Stat. Mech. Appl. **147**, 280 (1987).
[39] P. Wiltzius, Hydrodynamic Behavior of Fractal Aggregates, Phys. Rev. Lett. **58**, 710 (1987).
[40] M. Y. Lin, H. M. Lindsay, D. A. Weitz, R. C. Ball, R. Klein, and P. Meakin, Universality of fractal aggregates as probed by light-scattering, Proc. R. Soc. London Ser. A: Math. Phys. Eng. Sci. **423**, 71 (1989).
[41] J. Tate and G. Ward, Interferences in immunoassay, Clin. Biochem. Rev. **25**, 105 (2004).
[42] H. Du, P. Chandaroy, and S. W. Hui, Grafted poly-(ethylene glycol) on lipid surfaces inhibits protein adsorption and cell adhesion, Biochim. Biophys. Acta Biomembr. **1326**, 236 (1997).

[43] N. Parveen, S. Block, V. P. Zhdanov, G. E. Rydell, and F. Höök, Detachment of membrane bound virions by competitive ligand binding induced receptor depletion, Langmuir **33**, 4049 (2017).

[44] O. M. Szklarczyk, N. Gonzalez-Segredo, P. Kukura, A. Oppenheim, D. Choquet, V. Sandoghdar, A. Helenius, I. F. Sbalzarini, and H. Ewers, Receptor concentration and diffusivity control multivalent binding of Sv40 to membrane bilayers, PLoS Comput. Biol. **9**, e1003310 (2013).

[45] W. B. Turnbull, B. L. Precious, and S. W. Homans, Dissecting the cholera toxin-ganglioside GM1 interaction by isothermal titration calorimetry, PLoS Comput. Biol. **126**, 1047 (2004).